Fashion and Textiles

RESEARCH Open Access

Nondestructive quantitative model for predicting the residual tensile strength of silk textile cultural heritage based on machine learning

Seonghee Pak[1], Byoungho Ellie Jin[1,2] and Changsang Yun[1*]

*Correspondence:
cyun@ewha.ac.kr

[1] Department of Fashion Industry, Ewha Womans University, 52 Ewhayeodae-Gil, Seodaemun-Gu, Seoul 03760, Republic of Korea
[2] Wilson College of Textiles, North Carolina State University, 1020 Main Campus Drive, Raleigh, NC 27695, USA

Abstract

Silk is susceptible to deterioration induced by light, heat, and moisture, which leads to reduced structural stability and progressive strength loss. However, because destructive analysis is fundamentally unsuitable for silk textile cultural heritage, residual tensile strength is typically inferred through subjective evaluation. This study aims to quantitatively analyze deterioration behavior and examine the feasibility of nondestructive prediction of the residual tensile strength of silk textile cultural heritage by employing indicators that exhibit significant correlations with tensile strength reduction. As indicators of tensile strength, protein secondary structure, pH, moisture regain, yellow index, and K/S value were measured in artificially aged silk textiles. Results showed that tensile strength was not significantly influenced by differences in deterioration environments but correlated with crystallinity and protein secondary structure composition. Although linear regression demonstrated limited explanatory power ($R^2 = 0.576$), XGBoost demonstrated improved predictive performance ($R^2 = 0.654–0.751$) by capturing complex multivariate interactions, suggesting the potential for nondestructive estimation of residual tensile strength in textile cultural heritage. The prediction model using crystallinity, protein secondary structure contents, pH, yellow index, and K/S value showed the highest predictive accuracy. Further, with the accumulation of data encompassing textiles with diverse properties and the refinement of relevant indicators, the development of a machine learning–based nondestructive precision prediction model is anticipated. Such an approach can overcome the limitations of subjective assessment and contribute to systematic conservation management through the quantitative prediction of residual tensile strength in textile cultural heritage.

Keywords: Silk textile cultural heritage, Artificial deterioration, Residual tensile strength, Nondestructive prediction, Machine learning

© The Author(s) 2026. **Open Access** This article is licensed under a Creative Commons Attribution 4.0 International License, which permits use, sharing, adaptation, distribution and reproduction in any medium or format, as long as you give appropriate credit to the original author(s) and the source, provide a link to the Creative Commons licence, and indicate if changes were made. The images or other third party material in this article are included in the article's Creative Commons licence, unless indicated otherwise in a credit line to the material. If material is not included in the article's Creative Commons licence and your intended use is not permitted by statutory regulation or exceeds the permitted use, you will need to obtain permission directly from the copyright holder. To view a copy of this licence, visit http://creativecommons.org/licenses/by/4.0/.

Springer

Introduction

Silk is a material with evidence of use dating back approximately 6,000 years to the Neolithic era, and it has been used as a material in diverse cultural heritage throughout its long history. As an organic material, silk is susceptible to deterioration induced by light, heat, microorganisms, and other environmental factors, which reduces its structural stability and shortens its lifespan. Silk textile cultural heritage materials experience a reduction in strength as deterioration progresses, thereby increasing their susceptibility to damages such as creep, fracture and unraveling of seams; consequently, continuous monitoring is required to ensure stable preservation. However, silk often exhibits no obvious external changes even when deteriorating, and it does not deteriorate proportionally with time. Further, information on usage and storage environments that influence deterioration rates is often limited. Moreover, quantifying residual strength through tensile strength measurements constitutes a destructive analysis; thus, such approaches are fundamentally unsuitable for application in the cultural heritage field (Tanasescu et al., 2024).

The extent of damage to most silk textile cultural heritage is assessed by skilled conservators based on professional experience; however, objectively sharing and comparing condition states remain difficult because such assessments are typically recorded using subjective language. Beyond individual assessments, establishing objective metrics for tensile strength is crucial for multidisciplinary decision-making (Adriaens & Demortier, 2004). Quantified data serves as a common language among conservators, curators, and administrators, ensuring safety during the utilization of cultural heritage, such as long-term display planning and international loan exhibitions. To address these limitations, various non-destructive or micro-destructive analytical methods have been introduced to obtain quantitative data (Gong et al., 2022; Koperska et al., 2014, 2015a, 2015b; Vilaplana et al., 2015; Wang et al., 2025; Zhang & Yuan, 2010). A non-destructive and quantitative condition assessment protocol for weighted silk has been proposed (Anghelone et al., 2025), and a color change prediction model based on variables such as color difference and the degree of oxidation in silk has also been developed (Zhou et al., 2023a, 2023b). However, these studies have primarily focused on characterizing visible alterations or the degree of chemical degradation, leaving the quantitative prediction of residual tensile strength—a critical indicator for practical handling and preservation—largely unexplored.

Silk based artifacts, such as garments, socks, pouches and sitting cushions, are exposed to physical stress during exhibition, storage, and conservation treatment processes, requiring a clear quantitative assessment of residual tensile strength for safe handling (Park, 2019). Changes in the mechanical properties of silk, such as tensile strength reduction, can be explained by structural changes. Silk is a polypeptide comprising amino acids linked by peptide bonds and can be classified into secondary structural conformations, including α-helix, β-sheet, β-turn, and random coil. The α-helix adopts a helical conformation, whereas the β-sheet is characterized by extended, pleated strands (Chen & Imamura, 2003). The β-turn is a hairpin-like structural motif that induces a reversal in polypeptide chain direction and serves to connect the α-helix or β-sheet (Marcelino and Gierasch 2008). The random coil essentially refers to a disordered structure (Kovács & Bodor, 2023). Each secondary structure differs in molecular arrangement,

bond lengths, and amino acid composition ratios, and these characteristics change with material deterioration (Badillo-Sanchez et al., 2018; Zhou et al., 2023a, 2023b). Structural changes in proteins are closely linked to their secondary structure ratios, crystallinity, and amino acid composition. Because these characteristics can be quantified using non-destructive analysis (Garside & Wyeth, 2007; Gong et al., 2022; McGill et al., 2019; Zhang et al., 2019), it is feasible to predict residual mechanical strength without damaging the silk artifacts. By leveraging machine learning algorithms, this study aims to transform multi-dimensional non-destructive data into a predictive model capable of estimating the residual tensile strength of silk artifacts.

This study aims to analyze the deterioration characteristics of silk textiles artificially aged under controlled conditions by applying statistical analysis and machine learning to quantitatively derived data to explore the feasibility of nondestructive prediction of residual tensile strength. Silk textile artifacts were replaced with accelerated-aged silk samples, and characteristic indicators applicable to tensile strength prediction were derived to determine predictability. The selected accelerating factors for deterioration were ultraviolet (UV) light, heat, and indoor environments with glass windows, considering the references and museum environments. The protein secondary structure, moisture regain, pH, and color change were considered analytical parameters based on their anticipated strong correlations with tensile strength.

Materials and Methods

Samples

The silk samples used in this study were 100% silk fabrics (Bombyx mori, filament) that were neither bleached nor dyed. Six types of fabrics that differed in degumming status, weave type, density, yarn count, weight, and thickness were selected. Table 1 presents the characteristics of each sample. Preliminary experiments indicated that the chemical and structural degradation mechanisms exhibited qualitatively similar trends across the samples. To avoid potential data ambiguity arising from differences in degradation rates among samples and to clearly visualize the full progression of the deterioration behavior, sample F—which exhibited the most representative behavior among all samples—was selected as the representative model, and the results were presented accordingly. All data from sample F and the other five samples were fully utilized for statistical analysis and for constructing the dataset used in the machine learning model. Samples exposed in an indoor environment with glass windows were designated as W; those exposed to UV

Table 1 Silk fabric sample specification

Sample code	Fiber content	Yarn count (denier)	Density (counts; 5cm × 5cm)	Weave type	Weight (g/m^2)	Thickness (mm)
F	Silk (degum)	45 × 105	250 × 175	Plain	56	0.10
H	Silk (degum)	15 × 32	300 × 200	Plain	25	0.05
C	Silk (degum)	60 × 165	175 × 125	Plain	78	0.19
S	Silk (degum)	32 × 74	600 × 250	Satin	82	0.15
Cr	Silk (raw)	14 × 14	150 × 138	Plain	10	0.06
O	Silk (raw)	20 × 20	225 × 213	Plain	21	0.09

radiation in the UV-A region were designated as UV; and those subjected to heat stress were designated as DH, with the heat temperature shown before DH for differentiation.

Accelerated deterioration

Light stress in sunlit indoor environment

The indoor environment with glass windows was simulated by combining an inner filter (S. Boro, Atlas, USA) and an outer filter (Soda Lime, Atlas, USA) with a xenon arc lamp in a weathering tester (Ci4000 Weather-Ometer, Atlas, USA). The distance between the sample and the light source is approximately 30 cm. Light exposure was conducted using a xenon arc lamp with an irradiance of 1.20 W/m^2 at 420 nm. Detailed conditions were controlled to maintain a temperature of 100 °C and a relative humidity (RH) of 30% (ISO 105-B06, 2020b). Analyses were conducted at 0, 24, 72, 120, and 168 h to determine changes based on the cumulative stress exposure duration.

UV-A stress

Considering the low sunlight resistance of silk, a UV-A stress environment (400–315 nm) was created using a UV tester equipped with a UV-A 340 lamp. The given UV radiation was 0.77 W/m^2 (340 nm). The chamber's internal temperature was set to the device's maximum temperature (80 °C: UV2000, Atlas, USA), similar to the conditions of light stress in a sunlit indoor environment, and room humidity was controlled at 50% RH (Atlas material testing technology GmbH, 2024). To determine changes based on the cumulative stress exposure duration, analyses were performed at the following time points: 0, 24, 72, 120, and 168 h.

Heat stress

Heat stress was induced using an oven (OF-22GW, Jeio Tech, KOR). To evaluate the effect of temperature differences between light stress in a sunlit indoor environment and UV-A stress conditions on deterioration behavior, the minimum and maximum temperatures were set to 100 °C and 200 °C, respectively, considering the heat resistance of the samples (Ahn et al., 2014; Kim, 2014; Rockwood et al., 2011). Accordingly, the heat stress temperatures were set to 100, 150, and 200 °C and monitored at 0, 24, 72, 120, and 168 h. To ensure the stability of statistical analysis and machine learning models, the sample size was expanded by considering 125 and 175 °C temperatures. Under conditions of rapid tensile strength reduction, monitoring was conducted at 6, 12, 24, and 48 h and the experiment was terminated when the tensile strength converged to 0 N. Under conditions where the decrease in tensile strength was gradual, the stress application time was extended and the experiment was terminated when no notable changes were observed.

Characterization

Analysis of secondary structures for silk

Fourier transform infrared spectroscopy (FT-IR; Spectrum 3, Perkin Elmer, USA) is a nondestructive analysis method commonly accessible in museums. Under the conditions of attenuated total reflectance (ATR) mode, a diamond crystal, 32 scans, a spectrum resolution of 4 cm^{-1}, and a spectrum range of 4,000–650 cm^{-1}, measurements were repeated five times at different positions. FT-IR spectra were collected using Spectrum

IR (version 10.7.2.1630). Assuming identical infrared absorption coefficients for each FT-IR spectrum, the amide I–Ⅲ region (1,800–1,400 cm^{-1}) was extracted and normalized to compare trends. The normalization algorithm was used to adjust the absorbance values at both ends of the amide I and Ⅲ regions to zero and calibrated them to the same area. Based on Geminiani et al.'s (2024) study, spectral changes under deteriorated conditions were quantified as follows:

$$SR = \frac{A_{1625}}{A_{1618}} \tag{1}$$

where SR denotes the shift ratio of the amide I peak in the FT-IR spectrum, and A_{1625} and A_{1618} denote the absorbance at 1,625 and 1,618 cm^{-1}, respectively.

Following the approach reported by Lee et al. (2023), who obtained comparable trends using a deconvolution method, crystallinity was calculated as follows:

$$X_C(\%) = \frac{A_{1620}}{A_{1620} + A_{1645}} \times 100 \tag{2}$$

where X_C denotes the degree of crystallinity (%), A_{1620} denotes the absorbance at 1,620 cm^{-1} corresponding to the β-sheet structure, and A_{1645} denotes the absorbance at 1,645 cm^{-1} corresponding to the random coil structure.

The amide I region (1,580–1,720 cm^{-1}) was extracted from the collected spectra, followed by baseline correction. Fourier self-deconvolution was applied to the preprocessed spectra to resolve overlapping bands, yielding eight subpeaks (smoothing factor of 0.25, gamma function of 30.0). Curve fitting was performed until convergence was achieved based on the reduced chi-square criterion, with a convergence tolerance set to 10^{-5}. The relative content of each protein secondary structure was calculated as the percentage area of the corresponding subpeak relative to the total amide I band area. All spectral preprocessing and curve-fitting procedures were performed using OriginPro (version 10.1.5.132). The deconvolution results were assigned to each secondary structure as follows—side chain: 1,597–1,609 cm^{-1}; antiparallel β-sheet: 1,610–1,625 cm^{-1}; native β-sheet: 1,626–1,636 cm^{-1}; random coil: 1,637–1,655 cm^{-1}; α-helix: 1,656–1,662 cm^{-1}; β-turn: 1,663–1,696 cm^{-1}; and parallel β-sheet: 1,697–1,703 cm^{-1} (Zhou et al., 2001; Bucciarelli et al., 2021; Hu et al., 2006).

Tensile strength and hydrogen ion concentration

Tensile strength was measured using a universal testing machine (UNITEST M1, TEST ONE, KOR) according to ISO 13934-1:2013 with a gauge length of 75 mm, a crosshead speed of 50 mm/min, and a measurement unit of Newton (ISO 13934-1, 2013). Samples were prepared with a 60-mm width and 100-mm length, leaving frayed, ungripped margins of 5 mm on each side. Each sample was measured three times in the warp and weft directions, and the average value was calculated.

Hydrogen ion concentration was measured using a pH meter (Laqua pH/Ion Meter F-72, Horiba, JPN) (ISO 3071, 2020a). Owing to the impracticality of sampling 5×5-mm^2 samples from textile cultural heritages, the method was modified by applying deionized water (pH 5.0–7.0) directly to the sample surface. Each deterioration condition was measured five times, and the average value was calculated.

Moisture regain

Moisture regain was measured according to ASTM D2654-22. Reflecting typical museum conservation conditions for textile cultural heritage, samples were conditioned to moisture equilibrium at 20 ± 2 °C and 50% ± 5% RH using a chamber (PL-3KPH, ESPEC Corp., JPN; ASTM D1776, 2020b; Cultural Heritage Conservation Science Center, 2017; ICOM, n.d.; Ministry of Culture & Sports, 1996; National Museum of Korea, 2025; Seoul Museum of History, n.d.). Samples were dried in an oven (OF-50, Daihan Scientific Co., KOR) at 105 °C for at least 1.5 h. Moisture regain was determined when the mass change between successive weighing before and after drying was less than 0.1% (ASTM D2654-22, 2022). Measurements were performed using a precision balance (ARG423, Ohaus, USA), and the average value was calculated after repeating the experiment three times. Moisture regain was obtained using Eq. (3):

$$Moisture\ Regain(\%) = \frac{(C - B)}{B} \times 100 \tag{3}$$

where C denotes the mass of conditioned sample (g), and B denotes the mass of bone-dried sample (g).

Yellow index and K/S value

The surface color of yellowed samples due to deterioration was measured using a spectrophotometer (CM-700d, Konica Minolta, JPN) under D65 standard light source and 10° standard observer conditions; the yellow index was calculated using Eq. (4) (ASTM E313-20, 2020a). A total of 13 arbitrary points (one per 13 × 13-cm^2 area) were selected and measured. The yellowing tendency was determined using Eq. (5) as the difference in yellow index between the control and artificially deteriorated samples. Surface reflectance was measured at 10-nm intervals over the wavelength range of 360–740 nm, and the K/S values before and after treatment were calculated using the Kubelka–Munk equation described in Eq. (6).

$$\Delta YI = \frac{1.3013X_{CIE} - 1.1498Z_{CIE}}{Y_{CIE}} \times 100 \tag{4}$$

$$\Delta YI_{D-U} = YI_D - YI_U \tag{5}$$

$$K/S = (1 - R)^2 \div 2R \tag{6}$$

where X_{CIE}, Y_{CIE}, and Z_{CIE} denote the tristimulus values defined by the CIE XYZ color system in the X, Y, and Z directions, respectively; ΔYI denotes the yellow index, $\Delta YI_{D\text{-}U}$ denotes the yellowing tendency, YI_D denotes the yellow index of the treated sample, and YI_U denotes the yellow index of the untreated sample; and K denotes the abruption coefficient of the sample, S denotes the scattering coefficient of the sample, and R denotes the surface reflectance of the sample.

Statistical analysis and machine learning

Statistical analysis was conducted using IBM SPSS Statistics (version 29.0.1.0) to examine the correlation between the tensile strength and deterioration indicators and to

derive a correlation equation. The mean tensile strength values in the warp and weft directions of the samples were used as the dependent variable, and indicators that varied with deterioration were used as independent variables. Pearson's correlation analysis was performed to identify indicators that exhibited statistically significant correlations ($p < 0.05$). Regression analysis was then conducted using the statistically significant indicators as independent variables. The model fit was confirmed at tolerance > 0.100 and variance inflation factor (VIF) < 10.0.

The eXtreme Gradient Boosting (XGBoost) algorithm was selected based on the characteristics and objectives of the dataset. XGBoost was selected because it is effective for modeling non-linear relationships and interactions among variables, particularly in relatively small datasets. The model was implemented in a Jupyter Notebook environment using Python (version 3.12.3). To develop a prediction model, and the target variable was defined as the mean tensile strength in the warp and weft directions. Crystallinity, protein secondary structure contents, FT-IR (ATR) spectrum shift ratio, pH, moisture regain, yellow index, and K/S value were used as independent variables for analysis. The dataset consisted of 95 independent observations, where each data point represents a unique combination of fabric type and deterioration duration, ensuring that no repeated measurements from the same experimental condition were included. Prior to modeling, the data were preprocessed to ensure consistency across variables. The dataset was randomly divided into a training set (80%) and a test set (20%) (Lee et al., 2025). To optimize the model and ensure generalization performance, hyperparameter tuning was conducted using Randomized Search Cross-Validation on the training data. The predictive performance of the developed models was evaluated using the coefficient of determination (R^2), root mean square error (RMSE), mean absolute error (MAE), and mean absolute percentage error (MAPE) (Liu et al., 2024).

Results and Discussion

Changes in protein secondary structure during deterioration

The secondary structure changes in silk were nondestructively analyzed via ATR FT-IR analysis. Figure 1a shows the extracted amide I region (1,800–1,400 cm^{-1}). The overall absorbance tended to decrease as deterioration progressed. The peak positions and spectral profiles of the amide I region, associated with C=O stretching vibrations, as well as the amide II and III regions, primarily related to C–N stretching

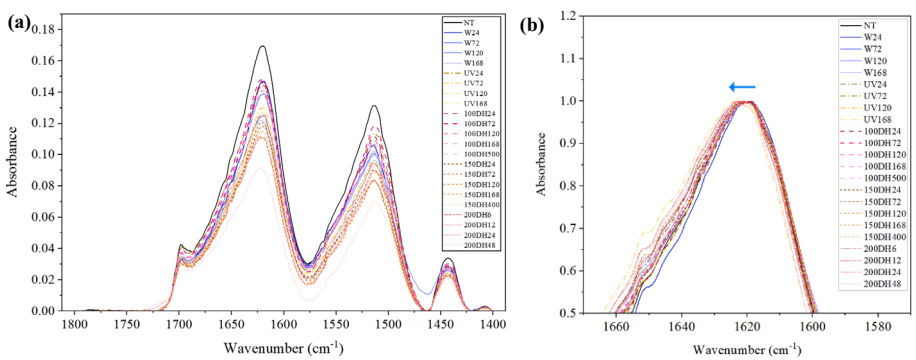


Fig. 1 FT-IR spectra of samples: **a** amide-related bands, and **b** normalized amide I peak shift

and N–H bending vibrations, remained largely unchanged regardless of the deterioration conditions. In addition, a slight peak shift was observed in the amide I region. Figure 1b shows the extracted and normalized amide I region, revealing a tendency for the amide I peak to shift toward higher wavenumbers as deterioration progressed. The blue shift is attributable to the C=O bond becoming relatively strengthened as hydrogen bonding weakens during the deterioration process. Moreover, the decrease in absorbance is attributable to a reduction in the C=O functional groups resulting from deterioration induced by light or heat stress. These results suggest that although the overall chemical composition of the samples remained unchanged, alterations occurred at the secondary structure level. Therefore, deconvolution was performed on the amide I region, which clearly correlates with secondary structure and vibration and is sensitive to changes in the structure, to compare changes in the relative content of secondary structural components (Belton et al., 2018; Bucciarelli et al., 2021). The analysis results are shown in Fig. 2a–d. In the early deterioration stages, the α-helix and random coil contents decreased whereas the β-sheet content increased. The α-helix and random coil primarily constitute the amorphous regions. Owing to their loose and disordered molecular arrangement (Pak & Kim, 2004; Zhou et al., 2023a, 2023b), these regions exhibit weaker intermolecular interactions and are hence more susceptible to deterioration than the crystalline regions. In addition, the initial increase in the β-sheet content may reflect a relative increase associated with the prior deterioration of amorphous regions rather than an absolute increase, as it is not accompanied by a corresponding increase in the β-turn content. Subsequently, the β-sheet content began to decrease after only 6 h under the 200DH condition, and a marked reduction in the β-sheet content was observed under the W and UV conditions. This decrease may be associated with a reduction in crystalline packing density resulting from the weakening of van der Waals interactions and hydrogen bonding

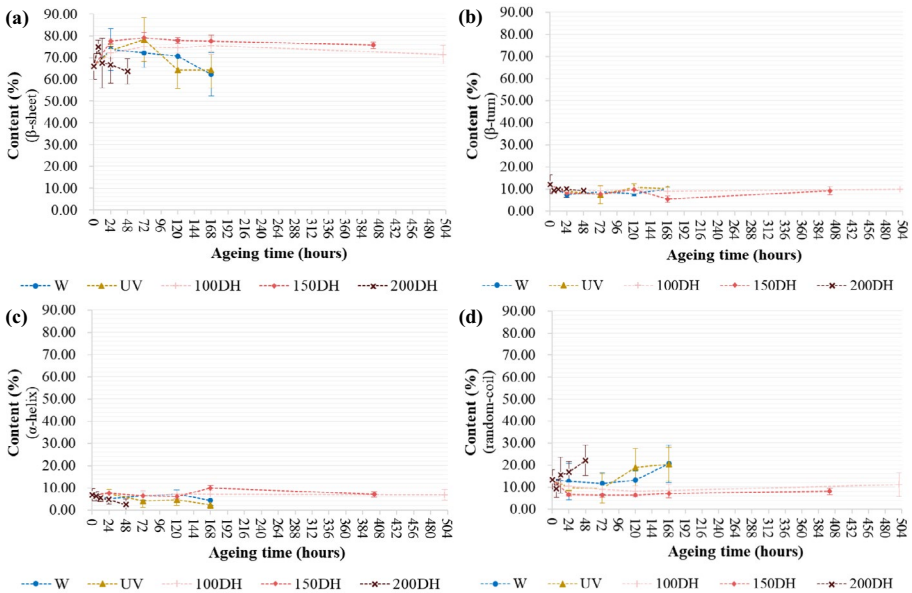


Fig. 2 Changes in protein secondary structure content under different deterioration conditions: **a** β-sheet content, **b** β-turn content, **c** α-helix content, and **d** random coil content

as well as deterioration. Under each deterioration condition, the β-sheet content decreased in the order of 200DH > W > UV > 150DH > 100DH. After increasing to approximately 75%–80%, the content began to decrease. This result is partially consistent with a previous study that reported the crystalline region of B. mori fibroin level to be up to 60%–70% (Sashina et al., 2006).

The relative changes in the secondary structure contents may reflect the distribution between crystalline and amorphous regions. Accordingly, they were quantified as crystalline and are shown in Fig. 3. The crystallinity of the untreated sample was 44.29%, and it increased to 45.71%–45.98%. This initial increase is attributed to the preferential decomposition of amorphous regions (random coil content), leading to a relative enrichment of crystalline β-sheet domains. However, this rising crystallinity does not indicate improved structural integrity; the concurrent blue shift in the Amide I band reflects weakening of inter-chain hydrogen bonds and the bond breakage, resulting in structural destabilization and reduced tensile strength despite the higher crystalline proportion. Similar interpretations have been reported in previous studies (Li et al., 2013, 2019).

Following this initial phase, no notable change was observed under most conditions, except for a decrease under W, UV and 200DH conditions. This tendency for crystallinity to stabilize or decrease after the initial increase reflects stage-dependent deterioration behavior, wherein the collapse of crystalline regions eventually proceeds after the preferential decomposition of amorphous regions.

Changes in tensile strength during deterioration

Figure 4 shows a comparison of the strength and elongation of samples deteriorated under W, UV, and DH conditions. Across all treatment groups, the strength and elongation exhibited a decreasing trend with increasing cumulative stress exposure duration. Unlike the untreated samples, the deteriorated samples showed a pronounced nonlinear deformation region (blue ellipse) before fracture. Similarities in this behavior suggest that differences in accelerated deteriorating factors do not cause differences in the fracture process. The tensile strength reduction rate was calculated for all samples using the same criteria; the results are shown in Fig. 5.

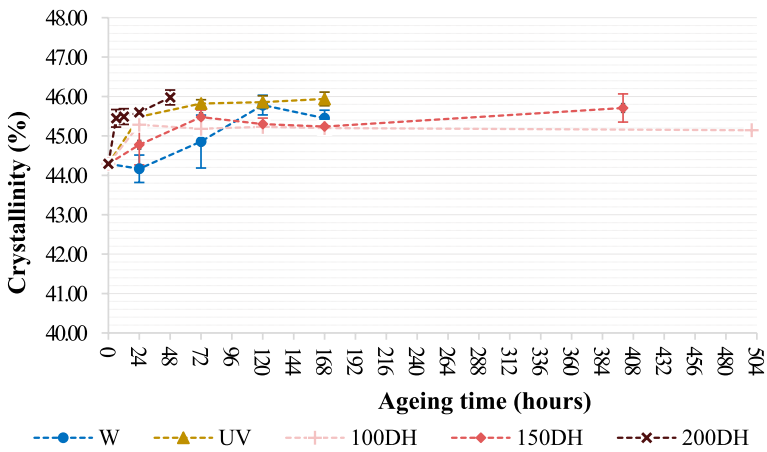


Fig. 3 Changes in crystallinity under different deterioration conditions

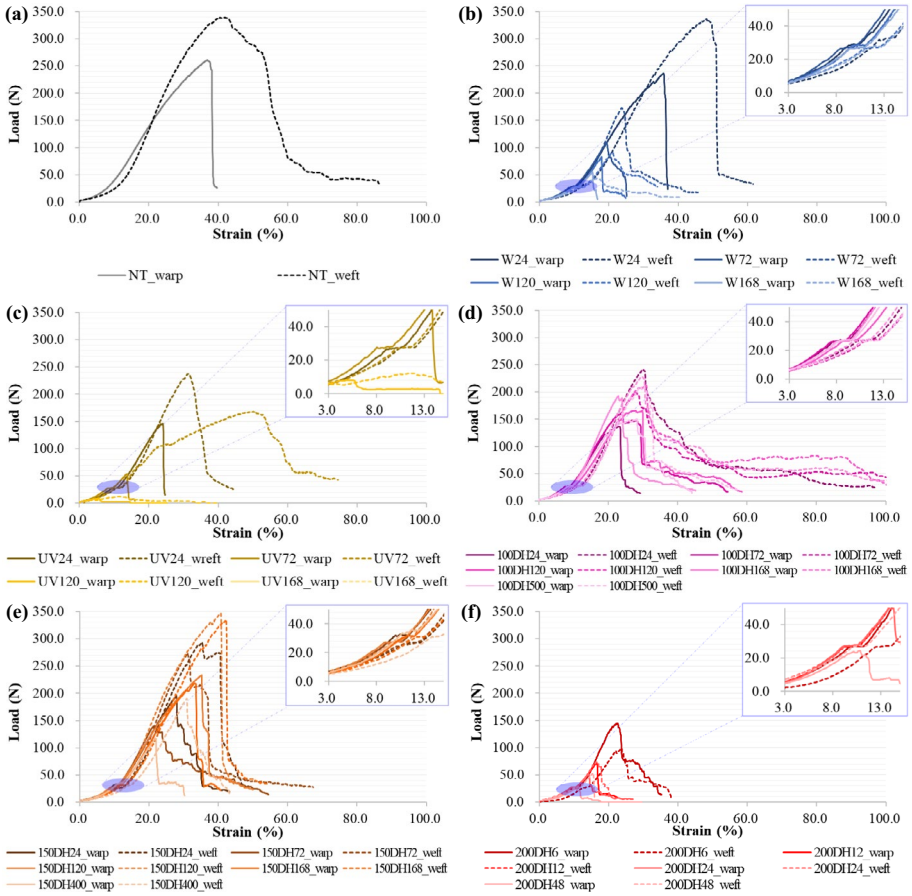


Fig. 4 Changes in tensile strength of silk deteriorated under various conditions: **a** untreated sample, **b** W sample, **c** UV-A sample, **d** 100DH sample, **e** 150DH sample, and **f** 200DH sample

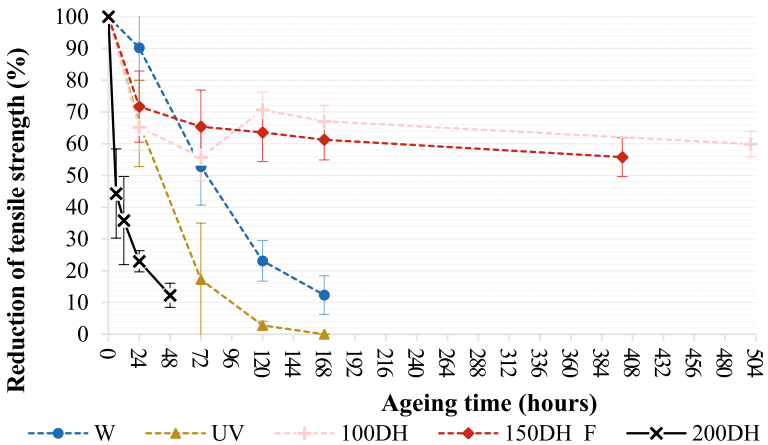


Fig. 5 Changes in tensile strength loss rate of silk deteriorated under various deterioration conditions

Tensile strength tended to decrease as stress accumulated. During deterioration, van der Waals forces and hydrogen bonds are broken, and α-helix, random coil, and β-sheet structures are damaged sequentially. In particular, β-sheets exist in a highly extended

form, imparting strong tensile strength to the fibers (Shen et al., 1998). Through hydrogen bonding, a close-packed structure is formed, creating a crystalline network that resists deformation under external forces (Yanagi et al., 2000; Zhao et al., 2021). Therefore, as deterioration progresses, the loss of tensile strength may be associated with a reduction in the bonding interactions that contribute to structural stability, along with a decrease in β-sheet content.

Tensile strength reduction also differed under various deterioration conditions. Tensile strength loss occurred most rapidly under the 200DH condition, whereas most tensile strength was lost after 168 h under the W and UV conditions. Meanwhile, only approximately 40.1% and 44.2% of tensile strength loss was measured under the 100DH and 150DH conditions, respectively, even after 168 h. Despite extending the processing time to 400 h, the reduction in strength remained below 50.0%. It is interpreted that deterioration due to dry heat reacts more sensitively to temperature increases than to the stress exposure duration.

Although the W and UV conditions involve light stress, they differ in terms of spectral distribution, distance from the light source, and chamber temperature and humidity. However, in the wavelength range to which silk fibers are most susceptible (233–355 nm), the W condition employs a filter that blocks radiation below 310 nm; therefore, the difference in spectral distribution between the two conditions is limited. Considering the observation under the 100DH condition, the results suggest that humidity and distance of the sample from the light source, rather than differences in internal chamber temperature, are more likely to have influenced the tensile strength reduction rate. Humidity is a factor that accelerates silk deterioration (Sharif & Esmaeili, 2017). The closer a sample is to the light source, the greater the transmitted light energy, which may have caused the difference.

Silk exhibits substantial variability in tensile strength due to its irregular cross-sectional area, thickness, and elongation rate. However, the standard deviation tended to decrease as deterioration progressed. This reduction in statistical variance suggests that the applied light or heat energy penetrated the fiber interior, inducing damage that caused tensile strength to converge toward lower levels. These results are consistent with the secondary structure analysis, which suggests a decrease in β-sheet content, known to contribute to the tensile properties of silk, after the breakdown of relatively weakly bound amorphous regions.

Changes in pH during deterioration

The pH of a sample was measured using deionized water at pH 7, assuming a neutral preservation environment and textile cultural heritage materials (Fig. 6). In the early deterioration stages, pH showed a sharp decrease followed by a gradual decline as the cumulative stress exposure duration increased. The pH of the untreated sample was 8.6. After 168 h of stress exposure, the pH decreased to 6.19, 5.24, 8.15, and 7.04 under the W, UV, 100DH, and 150DH conditions, respectively. The pH decreased most rapidly under the 200DH condition, reaching 6.62 within 48 h. The main component of silk, fibroin, has an isoelectric point of approximately 3.8–3.9 (Dang et al., 2010). Because the pH of the deionized water (pH 7.0) sprayed on the sample surface is higher than this value, fibroin may release hydrogen ions [H+], causing the pH to decrease. As deterioration

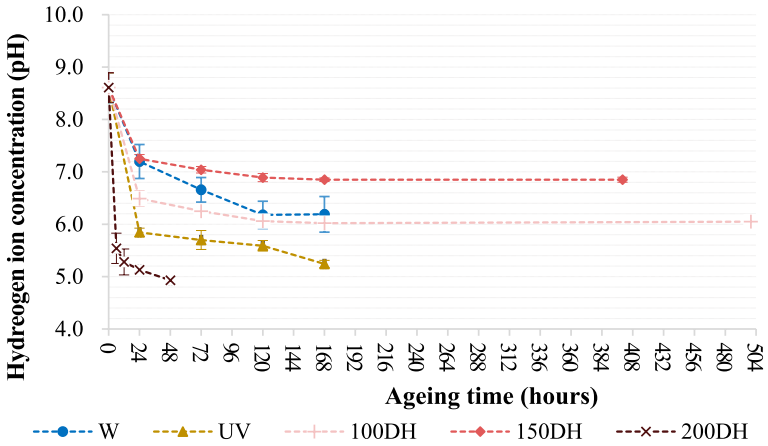


Fig. 6 Changes in pH under various deterioration conditions

progresses, the gradual decrease in pH is more likely attributable to chemical structural changes induced during the deterioration process rather than ion exchange stemming from the amphoteric nature of amino acids. Among the amino acids constituting fibroin, acidic amino acids (such as aspartic acid and glutamic acid) account for a relatively higher proportion than basic amino acids (such as arginine, histidine, and lysine); however, their abundance is still minor compared with neutral amino acids, such as glycine, alanine, and serine. Thus, Koperska et al., (2015a, 2015b) suggested that acidic products, such as phenols or carboxyl groups, generated during the deterioration process contributed to an increase in acidity. Garside and Wyeth (2007) reported that it resulted from increased exposure of acidic residues due to deterioration of the amorphous regions. A decrease in β-sheet content was observed under the 200DH and UV conditions, and the pH was relatively low. It is inferred that the carboxyl groups (–COOH) generated through main-chain hydrolysis, together with the deterioration of neutral amino acids, may have indirectly contributed to the observed pH changes.

Changes in moisture regain during deterioration

Changes in the moisture regain of the samples were expected due to alterations in the secondary structures by deterioration. Moisture regain was measured under museum conservation conditions (20 ± 4 °C, 50%–60% RH), and the results are shown in Fig. 7. The moisture regain of the untreated sample was 8.61%. After 24 h of stress exposure, the moisture regain decreased to 8.37%, 6.11%, 6.49%, and 7.25% under the W, UV, 100DH, and 150DH conditions, respectively. Under the 200DH condition, the moisture regain decreased to 5.54% within 6 h, exhibiting the most rapid decrease. This rapid decrease coincides with the stage characterized by reductions in α-helix and random coil content, suggesting a possible association with the reduction of the amorphous regions. As degradation progressed, a decrease in β-sheet content and an increase in random coil content were observed, as shown in Fig. 2. However, the corresponding increase in crystallinity remained limited to less than 1%, indicating a negligible effect on moisture regain. Therefore, these changes are likely more closely related to the reduction of hydrophilic groups or yellowing reactions, rather than being solely attributable to an increase in amorphous content. Although the crystalline regions undergo deterioration

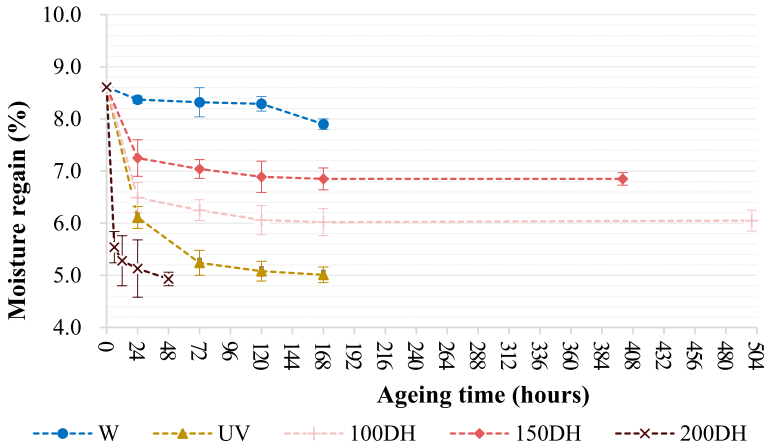


Fig. 7 Changes in moisture regain under various deterioration conditions

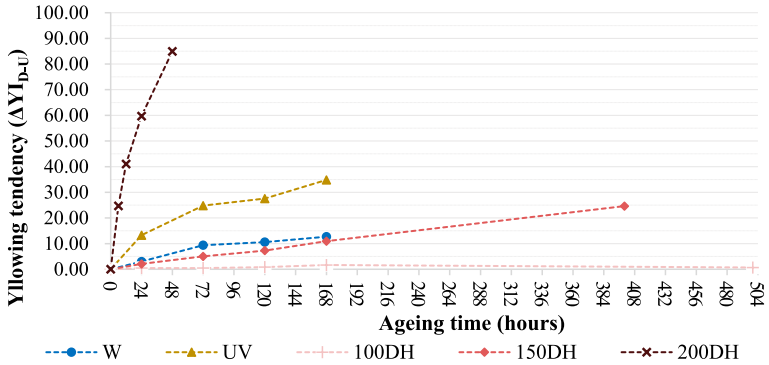


Fig. 8 Yellowing tendency under various deterioration conditions

accompanied by reduced molecular orientation, the continued decrease is primarily driven by a more pronounced reduction in hydrophilic functional groups, such as –COOH, $–NH_2$, and –OH, which can form hydrogen bonds or interactions with moisture (Otterburn, 1977). Meanwhile, the 100DH sample, which exhibited little deterioration of the crystalline regions even after 500 h, showed lower moisture regain than the W and 150DH samples, in which the crystalline region deteriorated more slowly. This is possibly because the amount of moisture penetrating the amorphous regions of silk is greater than that associated with hydrophilic functional groups and intermolecular crosslinking. The W and 150DH samples exhibited a relatively slower deterioration rate than the 200DH and UV samples, suggesting that the reduction in hydrophilic groups was insufficient to decrease the moisture regain.

Yellowing behavior during deterioration

Yellowing of textiles is a visible deterioration phenomenon, and changes in the yellowing index can be used to indirectly estimate changes in amino acid composition. Figure 8 shows the yellowing tendency derived after measuring the surface color of the samples under various deterioration conditions. The yellow index increased with the cumulative stress exposure duration, with the most rapid yellowing observed under the 200DH

condition. Under the 100DH condition, the yellow index remained below 5, indicating minimal yellowing. As the temperature decreased, the degree of yellowing diminished and its rate of increase slowed.

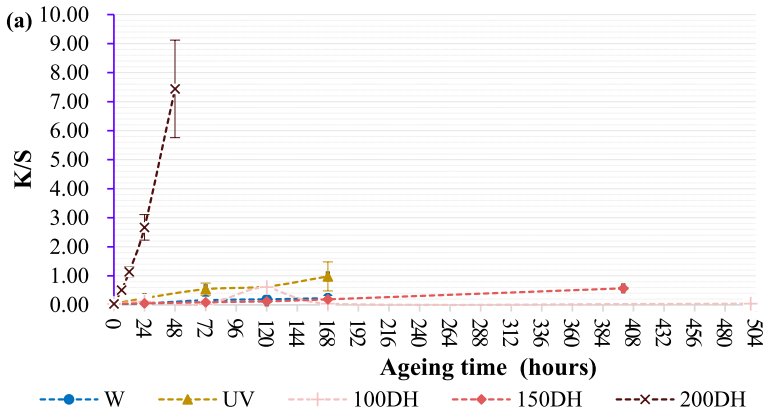
The oxidation of amino acids containing –OH groups and aromatic amino acids (such as tyrosine and tryptophan) is known to increase the yellow index (Hao et al., 2025; Kim et al., 2022). Consistently, high yellow indexes were observed under the 200DH and UV conditions, where a pronounced decrease in moisture regain was also detected. However, under the W condition, where moisture regain reduction was minimal, the yellow index was also low. Table 2 compares the yellow index, pH, and moisture regain based on tensile strength. The yellow index relative to tensile strength was higher under the UV condition than under the W condition, and it increased with temperature within the DH conditions. Except for tyrosine and tryptophan, most amino acids associated with yellowing primarily absorb UV radiation around 230 nm and exhibit negligible absorption in a longer-wavelength UV region (Pattison et al., 2012). Although UV-A and xenon arc lamps have different wavelength ranges, the spectral distributions in the UV region became similar due to the filters installed to simulate indoor environments. Another difference between the UV and W conditions is RH. Peptide bonds can undergo hydrolysis in environments containing moisture and heat, and the yellow index increases with RH (Luxford et al., 2009).

Yellowing is more sensitive to structural changes in the side chains, whereas the reduction in tensile strength is more closely related to main-chain scission. The difference between tensile strength loss and yellowness is therefore considered to arise from differences in the magnitude of energy and the duration of exposure. As the energy reaching the silk fiber decreases, the time required to affect the dense crystalline regions increases. Silk is highly susceptible to UV radiation; thus, both main-chain and side-chain degradation occurred within a short period, resulting in both strength loss and yellowness. In contrast, under the 150DH condition, even after 400 h of exposure, oxidation mainly affected the side chains, and the reduction in tensile strength was comparable to that observed after 72 h under the 100DH condition.

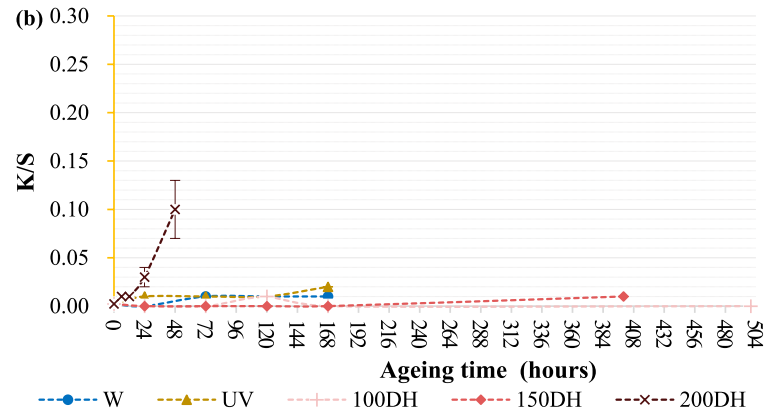
As the degree of yellowing in silk increased, the lightness (L*) decreased whereas the red (a*) and yellow (b*) chromatic components increased. These color-change characteristics were also confirmed by the K/S values calculated from the reflectance measurements at violet ($\lambda = 400$ nm) and yellow ($\lambda = 580$ nm) wavelengths. Figure 9 shows the variation in K/S values calculated for each phase. Compared with the untreated sample,

Table 2 Comparison of yellowness index, pH, and moisture regain in silk samples with similar tensile strength

Indicator sample	Tensile strength (N)	Yellow index	pH	Moisture regain (%)
UV72	51.50	31.16	5.70	5.24
200DH24	66.72	66.06	6.65	5.14
W120	66.78	16.95	6.18	8.29
W72	152.57	15.75	6.66	8.32
150DH400	181.53	30.98	6.13	6.85
100DH72	187.03	6.87	8.70	6.25



(a) λ = 400 nm



(b) λ = 580 nm

Fig. 9 Changes in color under different deterioration conditions: **a** λ = 400 nm, and **b** λ = 580 nm

the absorbance at 400 nm, corresponding to the violet region, exhibited the greatest change after yellowing. The increase in absorbed violet light increased the perceived yellowish tint of the object's color, and the reduced reflectance of short-wavelength light reduced the brightness. Meanwhile, the absorbance of yellow light increased somewhat 24 h after stress exposure; thus, an increase in red tint may be perceived by the naked eye.

Prediction models for tensile strength

Silk sequentially degraded from the amorphous to crystalline regions as it deteriorated, and crystallinity increased in the regions where the α-helix and random coil contents decreased. However, once a decrease in β-sheet content began, crystallinity also decreased. These internal structural variations were presumed to influence pH, moisture regain, and yellowing, thereby inducing changes. Accordingly, correlation analysis was conducted to elucidate the relationships among the measured properties and identify the factors exhibiting strong associations with the tensile strength reduction. The correlation analysis results are summarized in Table 3. Tensile strength exhibited statistically significant positive correlations with the β-sheet and α-helix contents ($p < 0.05$), whereas

Table 3 Correlation matrix between tensile strength and deterioration variables (n = 129)

Variables	Tensile strength	Crystal-linity	Shift ratio	β-sheet	α-helix	β-turn	Random coil	pH	Moisture regain	Yellow index	K/S value	Type of stress
Tensile strength	1											
Crystallinity	−0.175*	1										
Shift ratio	−0.378***	0.304***	1									
β-sheet	0.605***	−0.135	−0.035	1								
α-helix	0.345***	−0.238**	−0.120	0.337***	1							
β-turn	−0.569***	0.098	0.140	−0.668***	−0.054	1						
Random coil	−0.579***	0.230**	0.019	−0.914***	−0.644***	0.444***	1					
pH	0.102	−0.469***	−0.149	0.188*	0.132	0.026	−0.203*	1				
Moisture regain	0.112	−0.324***	−0.342***	−0.224*	0.167	0.216*	0.111	0.317***	1			
Yellow index	0.061	0.163	0.323***	0.278**	0.102	−0.322***	−0.252**	−0.101	−0.400***	1		
K/S value	0.044	0.080	0.180*	0.150	0.036	−0.231**	−0.135	−0.115	−0.341***	0.833***	1	
Type of stress	0.019	0.210*	0.200*	0.249**	−0.077	−0.182*	−0.141	0.116	−0.467***	0.564***	0.530***	1

* $p < 0.05$, ** $p < 0.01$, *** $p < 0.001$

significant negative correlations were observed with crystallinity, random coil content, β-turn content, and shift ratio ($p < 0.05$). Conversely, pH, moisture regain, yellow index, K/S value, and the type of stress accelerating deterioration did not show direct statistical significance with tensile strength ($p > 0.05$). However, pH showed a close association with variables that were significantly related to tensile strength, such as crystallinity, β-sheet content, and random coil content. This suggests that certain factors indirectly contribute to mechanical deterioration by mediating structural rearrangements. Therefore, multivariate analyses are required to further elucidate complex interactions and pathways beyond simple linear correlations.

Linear regression analysis was performed to specify the relationships between each set of variables. Regression models with different combinations of variables, constructed based on the observed correlations, are presented in Table 4. The regression models yielded a Durbin–Watson statistic of 1.109, and all VIFs were below 1.4, indicating negligible multicollinearity among the independent variables. The negative standardized coefficients observed for random coil content ($\beta = -0.423$) and β-turn content ($\beta = -0.375$) may suggest that the degradation of the amorphous regions is a major factor contributing to the reduction in tensile strength. In contrast, moisture regain exhibited a positive standardized coefficient ($\beta = 0.149$), which could be associated with relatively preserved amorphous regions in the samples, potentially resulting in a smaller decrease in tensile strength. This may be due to the fact that degradation of the amorphous regions reduces the available space for moisture penetration; thus, moisture regain could be considered a proxy indicator reflecting the extent of amorphous region degradation. Furthermore, the shift ratio of the amide I peak ($\beta = -0.266$) also showed a negative correlation, providing additional support for this interpretation. The model exhibited an explanatory power of 57.6% and was statistically significant ($F = 42.115$, $p < 0.001$). Even when different variables were selected, the increase in explanatory power was not significant. This was explained by the presence of nonlinear relationships and complex interactions among the variables, beyond simple linear relationships.

To comprehensively capture both linear and nonlinear relationships among multiple variables, the data processing approach was changed to machine learning. Each prediction model was constructed using different combinations of independent variables, and optimal hyperparameters were determined through Randomized Search Cross-Validation (CV). To maximize predictive precision and mitigate the risk of overfitting, CV was implemented as the primary optimization strategy. This approach facilitated the exploration of the hyperparameter space. The resulting performance metrics and hyperparameter settings for each model are summarized in Table 5. The R^2 of M1, which used only features with high Pearson's correlation coefficients, was 0.403. Meanwhile, M2, which incorporated all degradation-related indicators as identified in this study as being potentially associated with structural changes in silk related to tensile strength degradation, achieved an R^2 of 0.654, with corresponding decreases in RMSE, MAE, and MAPE. The improved performance of M2 suggests that the tensile strength of deteriorated silk fabrics is influenced by complex interactions among protein secondary structure, crystallinity, pH, moisture regain, yellowing, and absorbance at 400 nm. Based on this, the features were restructured based on their applicability in the cultural heritage field. Rather than relying solely on predictive performance as the criterion, a scenario reflecting the

Table 4 Linear regression analysis of factors influencing the decrease in tensile strength of artificially deteriorated silk

Variables	Coefficients			t	*p*	VIF	Model summary			
	B	SD	β				R2	Adj. R2	Std. error of the estimate	F
(Constant)	2481.479	511.529	–	4.851	< .001	–	0.576	0.562	92.316	42.115***
Shift ratio	− 2061.021	495.348	− 0.266	− 4.161	< 0.001	1.362				
β-turn	− 29.739	5.406	− 0.375	− 5.501	< 0.001	1.248				
Random coil	− 8.285	1.278	− 0.423	− 6.483	< 0.001	1.200				
Moisture regain	21.400	9.337	0.149	2.292	< 0.05	1.231				

* $p < 0.05$, ** $p < 0.01$, *** $p < 0.001$

Table 5 Optimized hyperparameters and predictive performance of machine learning models for tensile strength

Machine learning model	Statistical measure				Optimal value of hyperparameter					
	R2	RMSE	MAE	MAPE	n_estimators	learning rate	max depth	subsample	colsample_bytree	gamma
M1(H-Corr.)[1]	0.403	102.734	73.557	0.885	100	0.05	10	0.6	0.6	0.1
M2(full)[2]	0.654	78.210	53.327	0.720	150	0.10	3	0.6	0.6	0.0
M3(undyed)[3]	0.751	66.366	50.580	0.837	150	0.20	3	1.0	0.6	0.3
M4(small)[4]	0.686	74.527	56.322	0.503	100	0.05	5	0.8	0.6	0.3

Dependent variable: tensile strength

[1] Independent variables: crystallinity, shift-ratio, β-sheet, α-helix, β-turn, random coil

[2] Independent variables: crystallinity, shift-ratio, β-sheet, α-helix, β-turn, random coil, pH, moisture regain, yellow index, K/S value

[3] Independent variables: crystallinity, β-sheet, α-helix, random coil, pH, yellow index, K/S value

[4] Independent variables: shift-ratio, β-sheet, α-helix, random coil, pH

characteristics of textile cultural heritage in practical settings was assumed, in which textiles were categorized into colored and uncolored fabrics, with prediction models developed to suit each condition. M3 is a prediction model designed for application to undyed textile cultural heritage, in which the yellowing index can be reliably measured. This model exhibited the highest R^2 value (0.751), while the RMSE, MAE, and MAP were lowest. Because textile artifacts often involve small sample sizes that preclude reliable measurement of moisture regain, M4 represents an optimized combination of variables developed for such constrained conditions. By excluding the yellowing index and the K/S value, M4 may offer potential utility for predicting the residual strength of dyed fabrics.

Differences in predictive performance among M1–M4 arose not only from the number of features but also from differences in feature combinations. While linear regression analysis revealed strong individual associations between tensile strength and variables such as shift ratio, β-turn content, random coil content, and moisture regain, the highest predictive performance was achieved by M3, which included only a subset of these variables. In other words, the machine learning models demonstrated that predictive accuracy can be enhanced by considering combinations of variables, even when individual standardized coefficients are relatively modest. These results indicate that tensile strength degradation in silk cannot be attributed to a single dominant indicator, but is more effectively predicted through context-dependent combinations of degradation-related characteristics.

Conclusions

Silk textile cultural heritage experiences a decrease in tensile strength as deterioration progresses, increasing the risk of damage. However, because external changes are not readily apparent, immediate damage detection through visual inspection alone is difficult. This study aimed to analyze the correlation among tensile strength, secondary structure, pH, moisture regain, and color change in artificially deteriorated silk fabrics under various conditions. By constructing prediction models, it was sought to confirm the potential for nondestructive prediction of the residual tensile strength of silk fabrics.

The results showed that the tendency toward tensile strength reduction was not significantly influenced by differences in the deterioration stress type, specifically those created by variations in light and temperature. ($p > 0.05$); However, it tended to increase with the magnitude of applied energy, indicating that the amount rather than the type of energy governs the observed deterioration. In the early deterioration stages, the amorphous regions, including α-helix and random coil, were preferentially degraded, followed by the breakdown of the crystalline regions containing β-sheet. The pH and moisture regain also exhibited a rapid decrease at the onset of deterioration, followed by a gradual decline during the deterioration of the crystalline regions. The yellowing tendency increased sharply in the early stage. Among the conditions, UV exposure led to the second-fastest deterioration and the most pronounced yellowing, whereas the W condition exhibited a relatively low yellow index despite a reduction in tensile strength. Under DH conditions, the deterioration rate accelerated noticeably with increasing temperature, exhibiting nonlinear behavior wherein parameters such as β-sheet content and crystallinity increased to a maximum before decreasing, making it difficult to determine

the deterioration stage based solely on measurements taken at a single characteristic. Considering the relationships among these complex characteristics, applying machine learning algorithms that simultaneously reflect multiple variables improved prediction accuracy compared with traditional statistical analysis. Although the predictive performance of the present models ($R^2 = 0.403–0.751$) may not be sufficient to fully replace direct mechanical testing, they may still serve as useful references for risk assessment and conservation planning in textile conservation, where quantitative criteria or predictive models for evaluating mechanical strength remain limited. However, because the aging environments of cultural heritage in real contexts—such as during excavation—are inherently complex and highly variable, the present study is constrained by the use of controlled and reproducible artificial aging conditions. Nevertheless, expanding the indicator pool and integrating diverse datasets—including textiles with varying physical properties—will further enhance nondestructive predictive performance. This study achieved meaningful results for undyed silk fabrics and demonstrated the practical potential of the M4 model using a limited set of variables, future research is required to address complexities such as dye fading and to extend this methodology to other natural (e.g., wool, ramie) or man-made fiber. Future research will focus on refining quantitative machine learning models for the nondestructive prediction of tensile strength and developing practical guidelines for allowable loads. Such efforts will enable clearer discussions regarding acceptable levels of predictive error in subsequent applications, while also providing a foundation for systematic management strategies for the conservation and utilization of textile cultural heritage.

Acknowledgements
Not applicable.

Author contributions
SP conceptualized the study, performed the experiments, analyzed the data, and prepared the initial draft of the manuscript. BJ contributed to data analysis, interpreted the findings, and participated in manuscript writing and revision. CY oversaw the experimental design, evaluated the results, and provided guidance on manuscript preparation. All authors have read and approved the final version of the manuscript.

Funding
This work was supported by the Ewha Global Excellence Program Research Grant.

Availability of data and materials
The datasets used and/or analyzed during the current study are available from the corresponding author on reasonable request.

Declarations

Ethics approval and consent to participate
Not applicable.

Competing interests
Changsang Yun is an Executive Editor of Fashion and Textiles. Executive Editor status has no bearing on editorial consideration.

Received: 24 January 2026 Accepted: 11 May 2026
Published online: 26 May 2026

References

Adriaens, A., & Demortier, G. (2004). COST actions G1 and G8: EU programs on the use of radiation in art and archaeometry. *Nuclear Instruments and Methods in Physics Research Section B: Beam Interactions with Materials and Atoms, 226*(1–2), 3–9. https://doi.org/10.1016/j.nimb.2004.05.018

Ahn, C., Zeng, X., Li, L., & Obendorf, S. K. (2014). Thermal degradation of natural dyes and their analysis using HPLC-DAD-MS. *Fashion and Textiles*, *1*(1), 22. https://doi.org/10.1186/s40691-014-0022-5

American Society for Testing and Materials. (2020a). *Standard practice for calculating yellowness and whiteness indices from instrumentally measured color coordinates* (ASTM E313–20). https://store.astm.org/e0313-20.html

American Society for Testing and Materials. (2020b). *standard practice for conditioning and testing textiles* (ASTM D1776). https://store.astm.org/d1776_d1776m-16.html

American Society for Testing and Materials. (2022). *Standard test methods for moisture in textiles* (ASTM D2654–22). https://store.astm.org/d2654-22.html?_gl=1*1gjx3b9*_gcl_au*MTE2ODQzODg0Ni4xNzY1NTE4N DQ2

Anghelone, M., Dalhed, C., & Kimmel, T. (2025). Non-Destructive Condition and Damage Assessment of Historic Weighted Silk. *Fibers*, *13*(6), Article 78. https://doi.org/10.3390/fib13060078

Atlas material testing technology GmbH. (2024). *UVTest*. AMETEK. https://www.atlas-mts.com/products/standard-instruments/accelerated-uv-testing/uvtest

Badillo-Sanchez, D., Chelazzi, D., Giorgi, R., Cincinelli, A., & Baglioni, P. (2018). Characterization of the secondary structure of degummed *Bombyx mori* silk in modern and historical samples. *Polymer Degradation and Stability, 157*, 53–62. https://doi.org/10.1016/j.polymdegradstab.2018.09.022

Belton, D. J., Plowright, R., Kaplan, D. L., & Perry, C. C. (2018). A robust spectroscopic method for the determination of protein conformational composition–application to the annealing of silk. *Acta Biomaterialia, 73*, 355–364. https://doi.org/10.1016/j.actbio.2018.03.058

Bucciarelli, A., Greco, G., Corridori, I., Motta, A., & Pugno, N. M. (2021). Tidy dataset of the experimental design of the optimization of the alkali degumming process of *Bombyx mori* silk. *Data in Brief*, *38*, Article 107294. https://doi.org/10.1016/j.dib.2021.107294

Chen, J. Z., & Imamura, H. (2003). Universal model for α-helix and β-sheet structures in protein. *Physica a: Statistical Mechanics and Its Applications, 321*(1–2), 181–188. https://doi.org/10.1016/S0378-4371(02)01789-2

Cultural heritage conservation science center. (2017). *Cultural heritage handling manual*. National Research Institute of Cultural Heritage, 48.

Dang, Q., Lu, S., Yu, S., Sun, P., & Yuan, Z. (2010). Silk fibroin/montmorillonite nanocomposites: Effect of pH on the conformational transition and clay dispersion. *Biomacromolecules, 11*(7), 1796–1801. https://doi.org/10.1021/bm1002398

Garside, P., & Wyeth, P. (2007). Crystallinity and degradation of silk: Correlations between analytical signatures and physical condition on ageing. *Applied Physics A, 89*(4), 871–876. https://doi.org/10.1007/s00339-007-4218-z

Geminiani, L., Campione, F. P., Corti, C., Giussani, B., Gorla, G., Luraschi, M., Recchia, M., & Rampazzi, L. (2024). Historical silks: A novel method to evaluate their condition with ATR-FTIR spectroscopy and principal component analysis. *Journal of Cultural Heritage, 67*, 9–22. https://doi.org/10.1016/j.culher.2024.01.015

Gong, Y., Li, Z., Hu, J., Zhou, G., Xu, G., Yang, W., & Zhang, J. (2022). Insight into the measurements for determining the ageing degree of ancient silk. *Polymer Degradation and Stability*, *196*, Article 109833. https://doi.org/10.1016/j.polymdegradstab.2022.109833.

Hao, X., Wang, A., Ma, L., Li, H., Chen, B., Li, M., You, L. & Shen, X. (2025). Mechanism of copper ion-induced degradation of silk cultural relics: a multimodal analytical approach. *npj Heritage Science, 13*(1), Article 475. https://doi.org/10.1038/s40494-025-02035-9

Hu, X., Kaplan, D., & Cebe, P. (2006). Determining beta-sheet crystallinity in fibrous proteins by thermal analysis and infrared spectroscopy. *Macromolecules, 39*(18), 6161–6170. https://doi.org/10.1021/ma0610109

International Council of Museums [ICOM]. (n.d.). *Guidelines for costume*. ICOM International Committee for Museums and Collections of Costume, Fashion and Textiles. https://costume.mini.icom.museum

International Organization for Standardization. (2013). *Textiles - Tensile properties of fabrics; Part 1: Determination of maximum force and elongation at maximum force using the strip method* (ISO 13934–1:2013). https://www.iso.org/standard/60676.html

International Organization for Standardization. (2020a). *Textiles — determination of pH of aqueous extract* (ISO 3071:2020). https://www.iso.org/standard/74203.html

International Organization for Standardization. (2020b). *Textiles - tests for colour fastness; Part B06: Colour fastness and ageing to artificial light at high temperatures: Xenon arc fading lamp test* (ISO 105-B06:2020). https://www.iso.org/standard/63260.html

Kim, S. R. (2014). *Clothing materials* (3rd ed.). Kyomunsa.

Kim, Y. E., Bae, Y. J., Seok, Y. S., & Um, I. C. (2022). Effect of hot press time on the structure characteristics and mechanical properties of silk non-woven fabric. *International Journal of Industrial Entomology & Biomaterials, 44*(1), 12–20. https://doi.org/10.7852/ijie.2022.44.1.12

Koperska, M. A., Pawcenis, D., Bagniuk, J., Zaitz, M. M., Missori, M., Łojewski, T., & Łojewska, J. (2014). Degradation markers of fibroin in silk through infrared spectroscopy. *Polymer Degradation and Stability, 105*, 185–196. https://doi.org/10.1016/j.polymdegradstab.2014.04.008

Koperska, M. A., Łojewski, T., & Łojewska, J. (2015a). Evaluating degradation of silk's fibroin by attenuated total reflectance infrared spectroscopy: Case study of ancient banners from Polish collections. *Spectrochimica Acta Part a: Molecular and Biomolecular Spectroscopy, 135*, 576–582. https://doi.org/10.1016/j.saa.2014.05.030

Koperska, M. A., Pawcenis, D., Milczarek, J. M., Blachecki, A., Łojewski, T., & Łojewska, J. (2015b). Fibroin degradation–critical evaluation of conventional analytical methods. *Polymer Degradation and Stability, 120*, 357–367. https://doi.org/10.1016/j.polymdegradstab.2015.07.006

Kovács, D., & Bodor, A. (2023). The influence of random-coil chemical shifts on the assessment of structural propensities in folded proteins and IDPs. *RSC Advances, 13*(15), 10182–10203. https://doi.org/10.1021/ma0610109

Lee, J., Kim, J., & Lee, H. (2025). Diffusedesigner: sketch-based controllable clothing image generation. *Fashion and Textiles*, *12*(1), 26. https://doi.org/10.1186/s40691-025-00426-x

Lee, H. G., Lim, C. M., Kim, S. W., Kim, K. Y., & Um, I. C. (2023). Change of yellowing and crystallinity of silkworm variety cocoons by heat treatment. *Textile Science and Engineering, 60*(3), 178–186. https://doi.org/10.12772/TSE.2023.60.178

Li, M. Y., Zhao, Y., Tong, T., Hou, X. H., Fang, B. S., Wu, S. Q., Shen, X.-Y., & Tong, H. (2013). Study of the degradation mechanism of Chinese historic silk (*Bombyx mori*) for the purpose of conservation. *Polymer Degradation and Stability, 98*(3), 727–735. https://doi.org/10.1016/j.polymdegradstab.2012.12.021

108988 > Article 108988 Li, L., Decai, G., Zhengyuan, Y., & Jie, W. (2019). A preliminary study of the decline in solubility of ancient silk protein. *Polymer Degradation and Stability, 169*, 108988. https://doi.org/10.1016/j.polymdegradstab.2019.10898

13 > Article 13 Liu, S., Liu, Y. K., Lo, K. Y. C., & Kan, C. W. (2024). Intelligent techniques and optimization algorithms in textile colour management: A systematic review of applications and prediction accuracy. *Fashion and Textiles, 11*(1), 13. https://doi.org/10.1186/s40691-024-00375-x

Luxford, N., Thickett, D., & Wyeth, P. (2009). Preserving silk: Reassessing deterioration factors for historic silk artefacts. In: *Proceedings of the Combined (NZ and AUS) Conference of the Textile Institute*. 15–17 April 2009.

Marcelino, A. M. C., & Gierasch, L. M. (2008). Roles of β-turns in protein folding: From peptide models to protein engineering. *Biopolymers, 89*(5), 380–391. https://doi.org/10.1002/bip.20960

1800390 > Article 1800390 McGill, M., Holland, G. P., & Kaplan, D. L. (2019). Experimental methods for characterizing the secondary structure and thermal properties of silk proteins. *Macromolecular Rapid Communications, 40*(1), 1800390. https://doi.org/10.1002/marc.201800390

Ministry of Culture & Sports. (1996). *Research on environmental standards for museum exhibition and collections storage: Final Report*. Ministry of Culture & Sports. 380–381.

National Museum of Korea. (2025). *Status of the Storage Facility - Environmental Standards for Conservation Environment*. https://www.museum.go.kr/MUSEUM/contents/M0806020000.do

Otterburn, M. S. (1977). The chemistry and reactivity of silk. *Chemistry of natural protein fibers* (pp. 53–80). Springer US.

Pak, P. K., & Kim, C. Y. (2004). *Understanding of textile engineering*. Sigmaplus.

Park, S. (2019). An evaluation of the suitability of fluorescent fabrics and retroreflective materials for road traffic warning clothing in compliance with international standards. *Fashion and Textiles*, *6*(1), Article 34. https://doi.org/10.1186/s40691-019-0190-4

Pattison, D. I., Rahmanto, A. S., & Davies, M. J. (2012). Photo-oxidation of proteins. *Photochemical & Photobiological Sciences, 11*(1), 38–53. https://doi.org/10.1039/C1PP05164D

Rockwood, D. N., Preda, R. C., Yücel, T., Wang, X., Lovett, M. L., & Kaplan, D. L. (2011). Materials fabrication from *Bombyx mori* silk fibroin. *Nature Protocols, 6*(10), 1612–1631. https://doi.org/10.1038/nprot.2011.379

Sashina, E. S., Bochek, A. M., Novoselov, N. P., & Kirichenko, D. A. (2006). Structure and solubility of natural silk fibroin. *Russian Journal of Applied Chemistry, 79*(6), 869–876. https://doi.org/10.1134/S1070427206060012

Seoul Museum of History. (n.d.). *Museum Conservation Environment*. https://museum.seoul.go.kr/www/relic/cons/dataConssumculture/dataConssumMgr.jsp?sso=ok

Sharif, S., & Esmaeili, V. (2017). Effects of temperature and relative humidity on permanence of Buyid silk. *Journal of Cultural Heritage, 27*, 72–79. https://doi.org/10.1016/j.culher.2017.04.002

Shen, Y., Johnson, M. A., & Martin, D. C. (1998). Microstructural characterization of *Bombyx mori* silk fibers. *Macromolecules, 31*(25), 8857–8864. https://doi.org/10.1021/ma980281j

Tanasescu, E. C., Ene, A. G., Perdum, E., Iordache, O., & Secareanu, L. O. (2024). New fabric phase sorptive extraction for nondestructive analysis of heritage textile samples. *Heliyon*, *10*(10), Article e31020. https://doi.org/10.1016/j.heliyon.2024.e31020

Vilaplana, F., Nilsson, J., Sommer, D. V., & Karlsson, S. (2015). Analytical markers for silk degradation: Comparing historic silk and silk artificially aged in different environments. *Analytical and Bioanalytical Chemistry, 407*(5), 1433–1449. https://doi.org/10.1007/s00216-014-8361-z

Wang, Y., Chen, Q., Lei, Y., Kaya, M. G. A., Goh, K. L., & Tang, K. (2025). Identification, deterioration, and protection of organic cultural heritages from a modern perspective, *npj Heritage Science, 13*, Article 71. https://doi.org/10.1038/s40494-025-01601-5

Yanagi, Y., Kondo, Y., & Hirabayashi, K. (2000). Deterioration of silk fabrics and their crystallinity. *Textile Research Journal, 70*(10), 871–875. https://doi.org/10.1177/004051750007001005

Zhang, X., & Yuan, S. (2010). Measuring quantitatively the deterioration degree of ancient silk textiles by viscometry. *Chinese Journal of Chemistry, 28*(4), 656–662. https://doi.org/10.1002/cjoc.201090128

Zhang, X., Gong, D., & Gong, Y. (2019). Insight into the orientation behavior of thermal-aged and historic silk fabrics by polarized FTIR microspectroscopy. *Journal of Cultural Heritage, 38*, 53–63. https://doi.org/10.1016/j.culher.2019.02.007

Zhao, M., Qi, Z., Tao, X., Newkirk, C., Hu, X., & Lu, S. (2021). Chemical, thermal, time, and enzymatic stability of silk materials with silk I structure. *International Journal of Molecular Sciences*, *22*(8), Article 4136. https://doi.org/10.3390/ijms22084136

Zhou, C. Z., Confalonieri, F., Jacquet, M., Perasso, R., Li, Z. G., & Janin, J. (2001). Silk fibroin: Structural implications of a remarkable amino acid sequence. *Proteins: Structure, Function, and Bioinformatics, 44*(2), 119–122. https://doi.org/10.1002/prot.1078

Zhou, J., Zhou, X., Pan, L., Deng, Y., Zheng, H., Peng, Z., Wan, J., Zhou, Y., & Wang, B. (2023a). Molecular evidence of structural changes in silk using unlimited degradation mass spectrometry. *ACS Omega, 8*(38), 34410–34419. https://doi.org/10.1021/acsomega.3c02254

Zhou, X., Guo, Y., Luo, X., Zhang, L., Wu, M. & Zhang, W. (2023b). Systematic assessment of the silk deterioration behaviors for silk aging prediction. *Polymer Degradation and Stability*, *218*, 110532. https://doi.org/10.1016/j.polymdegradstab.2023.110532

Publisher's Note

Springer Nature remains neutral with regard to jurisdictional claims in published maps and institutional affiliations.

Seonghee Pak received a Ph.D. from the Department of Fashion Industry at Ewha Womans University in

2025.

Byoungho Ellie Jin is the Albert G. Myers Distinguished Professor in the Department of Textile and Apparel, Technology and Management at North Carolina State University. She is the founder and executive director of the Fashion and Textile Business Excellence Cooperative (FTBEC). Dr. Jin's research focuses on global fashion business, branding, consumer behavior, retailing, and innovative business models in the textile and apparel industries. She has published extensively in leading academic journals and has collaborated with scholars and industry professionals across multiple countries. Dr. Jin is the author of Global Fashion Business and serves as co-series editor of the Global Fashion Brand Management series. She is a Fellow and former President of the International Textile and Apparel Association.

Changsang Yun is an Associate Professor in the Department of Fashion Industry at Ewha Womans University. He received a Ph.D. from Seoul National University. His research group is to explore the textile-based science & technology for sustainable fashion.